Comparison of the Rotating Cylinder and Pipe Flow Tests for Flow-Sensitive Carbon Dioxide Corrosion

S. Nešić, G.T. Solvi, and J. Enerhaug***

ABSTRACT

The effects of various hydrodynamic parameters on the corrosion rate of low-carbon steel in carbon dioxide (CO_2) environments were studied. Two different flow geometries, rotating cylinder (RC) and pipe flow, were studied simultaneously in the same electrolyte within a glass loop. Comparisons were made over a wide range of parameters: temperature (T) = 20°C to 80°C, pH = 4 to 6, CO_2 partial pressure (P_{CO_2}) = 0 bar to 1 bar (0 kPa to 100 kPa), velocity (v) = 0 m/s to 13 m/s. The hydrodynamic conditions studied covered the range from static to highly turbulent flow. The corrosion process was monitored using polarization resistance, potentiodynamic sweep, and electrochemical impedance methods. The comparison of the two flow geometries was carried out in terms of hydrodynamics, mass transfer, and CO_2 corrosion. The measured mass transfer rates agreed well with published correlations for the RC and straight pipe (SP) flow. In the case of CO_2 corrosion, it was possible to achieve good agreement between corrosion rates in the two flow geometries at low temperatures by having the same water chemistry and mass-transfer conditions. This conclusion was valid for cases where no protective corrosion products, scale, or inhibitor films were present. However, at higher temperatures, films with a certain degree of protectiveness were observed. In those cases, lower corrosion rates were obtained on the SP specimen because of more dense and protective films.

KEY WORDS: carbon steel, carbon dioxide corrosion, corrosion rate, impedance, mass transfer, pipe flow, polarization resistance, potentiodynamic sweep, rotating cylinder

INTRODUCTION

Corrosion can be affected by flow differently depending on the mechanism governing the corrosion process. Two major cases can be distinguished: the effect of flow on corrosion when no surface films are present and the effect of flow on corrosion in the presence of surface films (precipitates, inhibitors, etc.).

In the absence of films, the primary effect of flow on corrosion is through mass transfer of the species involved in the corrosion reaction at the metal surface. For mass transfer in turbulent liquid flow, due to very large Schmidt numbers, all the concentration changes occur in a very narrow layer adjacent to the metal surface, deep within the viscous sublayer in the so-called mass-transfer boundary layer. The thickness of this layer is a function of the flow rate (Reynolds number) and flow geometry. Mass transfer usually is associated with limiting currents (i.e., with situations where the electrochemical processes at the metal surface proceed so fast that it is difficult to transport enough reactants from the bulk). Conversely, sufficiently rapid removal of corrosion products from the surface also can become limiting, which can lead to accumulation, (super)saturation and precipitation of surface films. However, if the

Submitted for publication December 1994. Presented as paper no. 130 at CORROSION/95, March 1995, Orlando, FL.

* Institutt for energiteknikk, P.O. Box 40, N-2007, Kjeller, Norway.
** Statoil, Postuttak, 7004 Trondheim, Norway.

0010-9312/95/000179/$5.00+$0.50/0

corrosion process is under charge transfer (activation) or chemical reaction rate control, changes in the flow and associated mass transfer will have no effect on the corrosion rate.

When surface films are present, they can reduce the corrosion rate by hindering the transport of species involved in the electrochemical reactions at the metal surface. In the case of inhibitor films, parts of the surface are "blocked" by the inhibitor, and the electrochemical double layer can be altered. The surface films can be removed locally or globally by chemical dissolution (in case of precipitates) or by mechanical forces, both of which lead to very high corrosion rates. Both mechanisms of film removal are related to flow and the transfer processes within. Chemical dissolution of surface deposits is related to mass transfer and to water chemistry. Mechanical removal of films is related to momentum transfer and often is encountered in single- and multiphase flows. In multiphase flow, film removal can be caused by the impact of solid particles present in the liquid, by the impact of droplets present in the gas flow (erosion), or by pressure and shear stress fluctuations due to slugging, etc. Even in single-phase flow, mechanical film removal often is seen particularly at geometrical irregularities (e.g., weld beads, grooves, and areas of sudden diameter changes). It is not yet clear which forces are responsible for mechanical film removal. In the literature, the average wall "shear stress"[1] and near-wall "turbulence fluctuations"[2] were connected with the onset of film removal. However, there has been no clear and detailed study where this was investigated.

The present study primarily was aimed at the effect of flow on carbon dioxide (CO_2) corrosion where protective surface films are not present. This probably is the simpler of the two cases discussed above. However, in high-temperature experiments of this work, films with a certain degree of protectiveness did form and were affected by the flow.

CO_2 corrosion, as studied here, is related to problems encountered in oil and gas production and transportation. The intention was to create an experimental setup where real-life conditions would be simulated as accurately as possible. However, simulation of field conditions in the laboratory is extremely complicated and primarily is dependent upon detailed knowledge of the processes occurring (both flow and corrosion). The processes occurring in the present system were so complicated that a simple scaling parameter most probably did not exist. This meant that successful transfer of data from one laboratory system to another and, further, to the field was possible only via a model describing the processes occurring. Therefore, the fruitless literature search for a single scaling flow parameter (Reynolds number,[3] shear stress,[4-5] turbulence,[2] etc.) that would capture the effect of flow on corrosion had little chance of success.

Nevertheless, a way to predict what would happen in field conditions is needed. One way would be to use complicated, high-pressure, multiphase flow loops.

With more knowledge of the processes, a small-scale apparatus can be sufficient. This study was concerned much with the transfer of data from one laboratory scale flow-corrosion system (rotating cylinder [RC]) to another (pipe flow) and ultimately to the field.

EXPERIMENTAL

Loop

The experimental glass flow loop used in the present study is shown in Figure 1. The loop was built to handle two-phase water and oil flow. However, only results from the single-phase water flow experiments are presented. Glass was selected as the main loop material for two reasons: It enabled application of aggressive cleaning procedures (in between experiments with inhibitors), and because it was optically transparent (important especially in two-phase flow).

Two test sections were mounted in the loop — the straight pipe (SP) and the RC. The same electrolyte was circulated through both test sections to guarantee identical water chemistries for the corrosion processes. The same idea was used previously by Efird, et al.[6] The enlarged view of the SP test section made from polytetrafluoroethylene (PTFE) is shown in Figure 2. Three steel specimens were flush mounted in the pipe (diam [d_p] = 15 mm [0.59 in.] inner diam [ID]). Up to three additional pipe test sections could be added to the existing one in series. The RC (diam [d_c] = 10 mm [0.394 in.]) mounted in a cylindrical glass chamber with all the measuring equipment is shown in Figure 3.

Most of the components of the loop, including the valves, were made form borosilicate glass and PTFE. Some minor components (mostly fittings) were made from polypropylene (PP), polyvinyl chloride (PVC), polyvinylidene fluoride (PVDF), rubber, type 316 SS (UNS S31600)[(1)] and C-276 steel (UNS N10276). The construction of the loop enabled reliable control of the flow parameters, water chemistry and temperature, and stable and reliable automatic operation of the loop for extended periods of time (up to several weeks).

Water Chemistry

Water chemistry is one of the most important factors affecting the corrosion rate, so significant

[(1)] UNS numbers are listed in *Metals and Alloys in the Unified Numbering System*, published by the Society of Automotive Engineers (SAE) and cosponsored by ASTM.

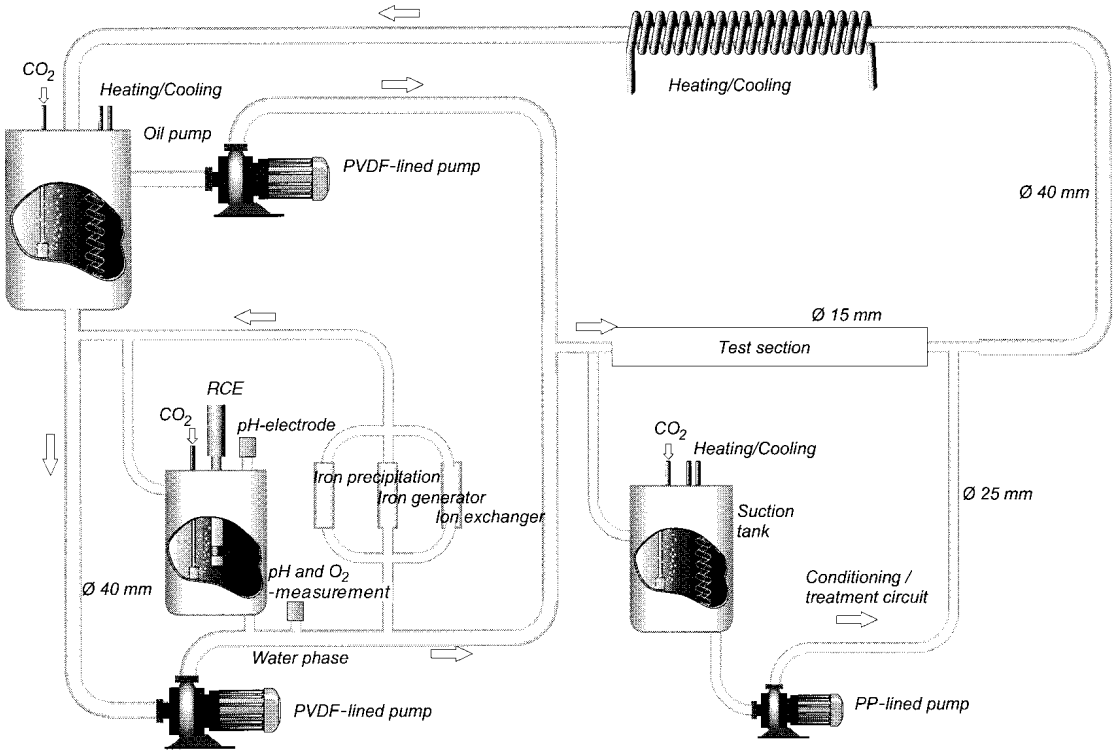

FIGURE 1. *Schematic of the glass flow loop.*

attention was given to this matter. Water preparation included: water purification by distillation or reverse osmosis and bubbling with CO_2 typically for 1 day prior to the experiment. Continuous CO_2 bubbling was maintained throughout the experiment. The oxygen (O_2) content was measured continuously and kept < 40 ppb throughout the experiment. Hydrochloric acid (HCl) and sodium bicarbonate ($NaHCO_3$) were added to achieve the desired pH. It was possible to control the concentration of iron cations (Fe^{2+}) by using an iron generator (to increase the Fe^{2+} concentration), an ion exchanger (which could substitute Fe^{2+} in the solution with hydrogen [H^+] or sodium [Na^+] ions), and a high-temperature iron precipitator. Typically once a day, samples of the loop water were taken for analysis to determine the amount of dissolved CO_2 and the concentration of Fe^{2+}.

The pH was measured with two independent electrodes to register a possible drift. One electrode was placed in a side stream taken from the main circulation circuit, and the other was placed in the RC chamber. When the discrepancy in the readings on the two pH meters was > 0.1, the electrodes were taken out, recalibrated, and eventually replaced. The water temperature was kept constant within ± 0.5°C in the range 20°C to 80°C.

Material

In all experiments, the steel tested was a low-carbon API 5L Grade X-65 steel,[2] a typical pipeline steel. Chemical composition of the steel is given in Table 1.

Corrosion Measurements

The corrosion process was followed using the electrochemical techniques of polarization resistance, alternating current (AC) impedance, and potentiodynamic sweep. A three-electrode setup was used in all electrochemical experiments, both in the SP and the RC test sections. In the SP test section (Figure 2), the working and the counter electrode were mounted flush with the pipe wall so that minimal flow disturbance was created. The working electrode made from carbon steel and the counter electrode made from C-276 steel were identical in shape (area [AA] = 2.9 cm^2 [0.45 $in.^2$]) and were mounted diametrically opposite each other so that a symmetrical current distribution was obtained during polarization experiments. An external silver-silver chloride (Ag-AgCl) reference electrode (filled with saturated potassium chloride [KCl]) was connected to the cell with an ion-conducting porous wooden plug.

In the RC test section (Figure 3), a carbon steel working electrode was mounted onto a rotator with a speed control unit (0 rpm to 5,000 rpm). The specimen was machined from the parent material into a

[2] American Petroleum Institute, 1220 L. St., N.W., Washington, DC, 20005.

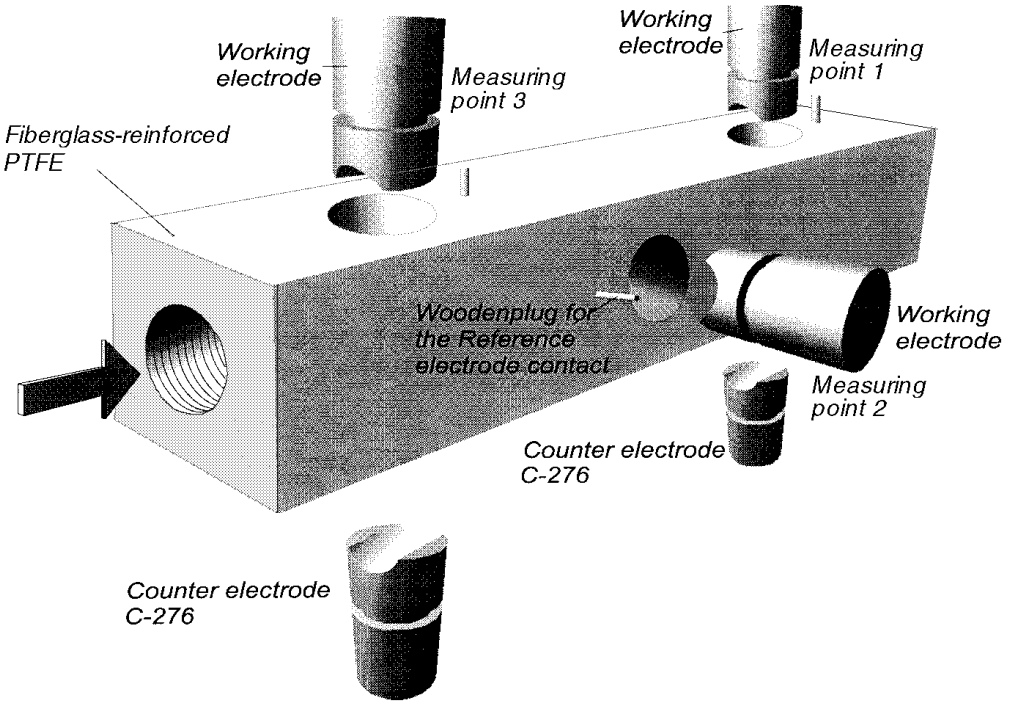

FIGURE 2. *Schematic of the SP test section made from PTFE.*

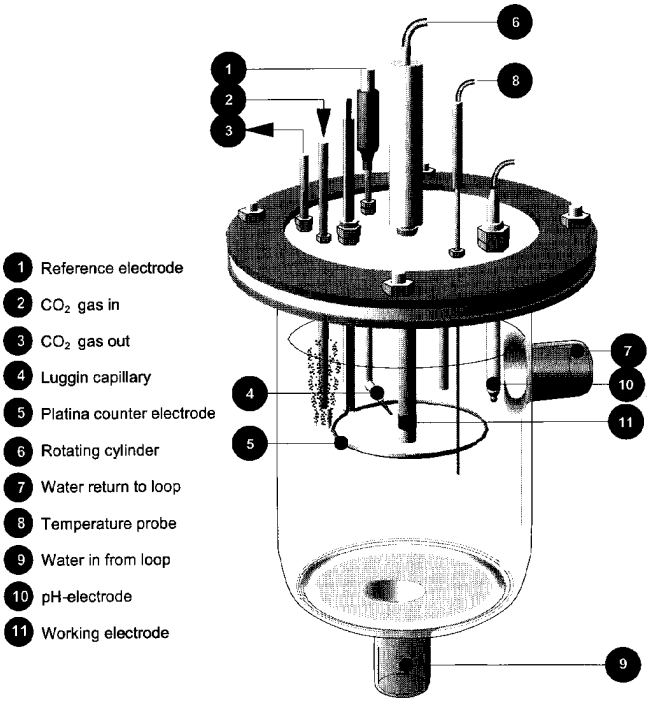

FIGURE 3. *Schematic of the RC test section made from glass.*

cylinder 10 mm (0.394 in.) in diameter and 10 mm (0.394 in.) long. The exposed area of the specimen was 3.14 cm^2 (0.49 $in.^2$) concentric platinum wire ring served as a counter electrode. An external Ag-AgCl reference electrode was connected to the cell using a Luggin capillary with a porous wooden plug. The rotating speed of the working electrode was controlled occasionally using a stroboscope. Electrochemical measurements were made using a potentiostat with an eight-channel multiplexer connected to a 486/25 mHz personal computer.

Procedure

The glass loop was filled with ≈ 56 L (14.8 gal) of electrolyte: distilled water + 1 mass% sodium chloride (NaCl). Then, the CO_2 was bubbled continuously through the electrolyte (usually for 24 h prior to the experiment) to deoxygenate and saturate the solution. Monitoring of pH and O_2 concentration was used to judge when the solution was in equilibrium. Then, the pH was adjusted by adding HCl or $NaHCO_3$. Prior to immersion, the carbon steel specimen surfaces were polished using 500- and 1,000-grit silicon carbide (SiC) paper, degreased with acetone, and washed with alcohol.

The polarization resistance measurements were conducted by polarizing the working electrode ± 5 mV from the free corrosion potential and scanning at 0.1 mV/s. The solution resistance was measured independently using AC impedance and subtracted from the polarization resistance. The AC impedance measurements were made by applying an oscillating potential to the working electrode ± 5 mV around the free corrosion potential using the frequency range 1 mHz to 100 kHz. At the end of each experiment, the potentiodynamic sweeps were

TABLE 1
Chemical Composition of the X-65 Pipeline Steel Used for the Working Electrode (mass%)

C	Mn	Si	P	S	Cr	Cu	Ni	Mo	Al	V	Sn	Ti	Nb
0.064	1.54	0.25	0.013	0.001	0.05	0.04	0.04	0.07	0.041	0.035	0.002	0.002	0.041

TABLE 2
Experimental Parameters

Test solution	1 mass% NaCl
Temperature	20°C to 80°C
Pressure	1 bar CO_2
pH	4 to 6
Dissolved oxygen	< 40 ppb
Velocity in pipe	Static – 13 m/s
Rotating speed	Static – 5,000 rpm
Test duration	1 to 7 days
Sweep rate	0.1 mV/s
Potentiodynamic sweep limits	–600 mV to 150 mV vs E_{oc}
AC impedance	±5 mV vs E_{oc} from 1 mHz to 100 kHz
Polarization resistance sweep limits	–5 mV to 5 mV vs E_{oc}

conducted, starting 600 mV below and finishing 150 mV over the free corrosion potential. The typical scanning rate used was 0.1 mV/s. Experimental conditions are summarized in Table 2. After removing the specimens from the loop, they were prepared for inspection by scanning electron microscopy (SEM) and energy dispersive x-ray analysis (EDXA).

Difficulties

Numerous difficulties followed the experimental program. Even very small quantities of contamination leaking from loop components were found to be detrimental and capable of leading to erroneous measurements. Lead contamination was encountered, with lead dissolving from a minute seal in a rotameter used to monitor the flow rate through a bypass stream. It was found that tin was dissolving from a graphite pump bearing. In both cases, the contaminating metals were deposited on the surface of the present specimen. The most serious contamination was discovered to come from a short nitrile rubber hose used to connect the pumps with the loop. The mysterious contaminant was a very effective corrosion inhibitor. All previous sources of contamination had to be removed before meaningful measurements could be made.

RESULTS AND DISCUSSION

Selection of an adequate laboratory scale apparatus for testing flow effects in CO_2 corrosion is a difficult task. The selected experimental setup must have well-defined hydrodynamic and mass-transfer characteristics. In addition, good control of water chemistry must be possible. The SP and RC test sections used in the present experiments satisfied both requirements. By testing the two flow geometries using the same electrolyte, it could be assumed that water chemistry was identical, and the work could be focused on the differences in the CO_2 corrosion process that arose from hydrodynamic and mass-transfer considerations.

The choice of the SP test section for a principal test geometry required no special justification: The practical importance and resemblance of this geometry to real systems is obvious. In addition, hydrodynamics and mass transfer in turbulent pipe flow have been investigated thoroughly, both experimentally and theoretically.[7]

A rotating disc first was considered instead of the RC because of its well-defined hydrodynamics and mass transfer.[8] However, as a rotating disc is primarily suitable for laminar flow studies, the RC geometry was selected. It enabled studies of turbulent flow and provided very uniform current distribution. In addition, detailed hydrodynamic and mass-transfer studies of the RC flow geometry could be found in the literature.[9-10]

Before proceeding with comparisons of the two flow geometries in terms of hydrodynamics, mass transfer, and corrosion, it might be useful to summarize what is known about the mechanisms of the CO_2 corrosion process. Figure 4, generated with an electrochemical model of CO_2 corrosion, illustrates this explanation.[11] When CO_2 is added to an aqueous solution, it is hydrated and forms a weak carbonic acid (H_2CO_3). Typically, only a very small proportion (0.25%) of dissolved CO_2 is hydrated into H_2CO_3. In addition, this is a slow process. H_2CO_3, as any other weak acid, provides a source of H^+ ions at a given pH.

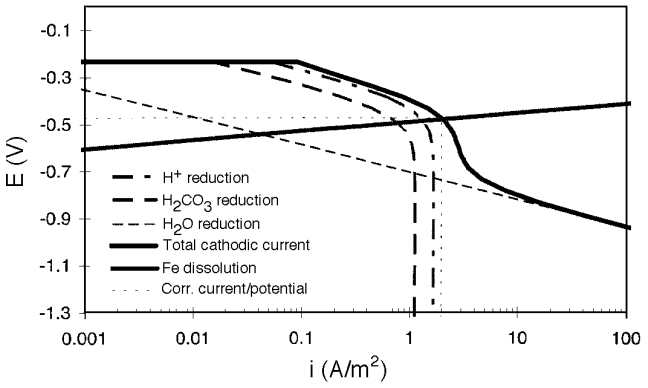

FIGURE 4. *Most important electrochemical reactions in CO_2 corrosion at pH 4, 20°C, 1 m/s, 1 bar CO_2.*

In an acidic solution, the reduction of H^+ is usually the most important cathodic reaction. It has been shown previously that the rate limiting step in the H^+ reduction reaction can be the diffusion rate of H^+ ions from the bulk of the fluid to the surface.[12] At higher pH values, the availability of H^+ ions decreases, and other competing cathodic reactions become important.

In CO_2 systems at low pH (pH < 4), there are so many H^+ ions that the H^+ reduction is still the dominant cathodic reaction. At intermediate pH (4 < pH < 6, the range of the primary present interest) in addition to the H^+ reduction a new cathodic reaction becomes important: the direct reduction of H_2CO_3. This additional cathodic reaction often is seen as the cause for CO_2 solutions to be more corrosive than pH alone would suggest. The reduction of H_2CO_3 can be under activation (charge-transfer) control[13] or under chemical reaction control[14-15] when the slow hydration step limits the rate of the overall reaction. At currents higher than the limiting for H^+ or H_2CO_3 reduction, the dominant cathodic reaction changes to direct reduction of water.[16] The governing mechanism depends on where the anodic and cathodic lines intersect.

In water-CO_2 corroding systems, it most often has been assumed that the sequence of anodic dissolution of iron is the same as it is in other acids[13,17] (i.e., the pH-dependent mechanism proposed by Bockris, et al.[18]). However, some recent findings[11,19] do not support this assumption. It seems that the iron dissolution reaction in CO_2-containing solutions proceeds without the influence of pH (for 4 < pH < 6).

Fluid Flow

From a practical point of view, turbulent flow regimes are of the primary interest. For pipe flow at Reynolds numbers below $Re_p = v_p d_p/\nu = 2{,}000$ (where v_p is velocity in m/s, d_p is pipe diameter in m/s, and ν is the kinematic viscosity in m^2/s), laminar flow is encountered. For $2{,}000 < Re_p < 3{,}000$, transition to turbulent flow occurs. Translated to the present experimental conditions (d_p = 15 mm ID, T = 20°C) turbulent flow was achieved for all velocities > 0.2 m/s. At higher temperatures, the transition occurred at even lower velocities. For a RC geometry, laminar flow typically is encountered for Reynolds numbers $Re_c = v_c d_c/\nu < 200$ (where $v_c = \omega d_c/2$ is the peripheral velocity of the RC, the rotational [angular] speed in rad/s, and d_c is the cylinder diameter in m). This means that in the present conditions (d_c = 10 mm, T = 20°C), already for rotation speeds > ω = 40 rpm, turbulent flow was encountered in the vicinity of the cylinder. This corresponded to a RC peripheral velocity of v_c = 0.02 m/s.

Turbulent flow in the two geometries has many similarities. Fully developed turbulence is encountered in the bulk liquid. As solid walls are approached, the turbulent fluctuations are damped so there exists a layer near the metal surface where viscous forces dominate and any turbulence is dissipated rapidly. Between this so-called viscous sublayer and the turbulent core, there is a transition layer, often called the buffer sublayer, where the viscous and turbulent forces are of the same order of magnitude. For aqueous systems which typically have large Schmidt numbers ($Sc \approx 10^3$), the mass-transfer boundary layer is very thin and is imbedded deeply into the viscous sublayer.

The shear stress exerted at the wall in pipe flow can be determined from the pressure gradient along a pipe by:

$$\tau_w = \frac{\Delta p}{\Delta L}\frac{d_p}{4} \qquad (1)$$

where τ_w is the wall shear stress in Pa and $\Delta p/\Delta L$ is the pressure drop along the pipe. However, the pressure drop was not measured in the experiments so the shear stress had to be determined from existing correlations. For turbulent pipe flow, such a relationship can be found only empirically in terms of laws of friction. One of the simplest such correlations is the Blasius equation:[7]

$$f_p = 0.079\,Re_p^{-0.25} \text{ for } Re_p > 3{,}000 \qquad (2)$$

where $f = 2\tau_w/\rho v^2$ is the Fanning friction factor and ρ is the density in kg/m^3. However, for high Reynolds numbers ($Re_p > 10^5$) this formula is in error. It is then most appropriate to use the Coolebrook equation:[20]

$$\frac{1}{\sqrt{f_p}} = -4\log\left(\frac{\varepsilon}{3.7d_p} + \frac{1.256}{Re_p\sqrt{f_p}}\right) \text{ for } Re_p > 3{,}000 \qquad (3)$$

which for smooth pipes ($\varepsilon/d_p = 0$) reduces to Prandtl's

universal law of friction:[7]

$$\frac{1}{\sqrt{f_p}} = 4\log\left(\mathrm{Re}_p\sqrt{f_p}\right) - 0.4 \text{ for } \mathrm{Re}_p > 3{,}000 \qquad (4)$$

and for very rough pipes to von Karman's equation:[7]

$$\frac{1}{\sqrt{f_p}} = 4\log\left(\frac{d_p}{\varepsilon}\right) + 2.28 \text{ for } \frac{d_p/\varepsilon}{\mathrm{Re}_p\sqrt{f}} < 0.01 \qquad (5)$$

For the RC in the case of a turbulent flow regime (smooth surfaces), the friction factor is:[10]

$$f_c = 0.158\,\mathrm{Re}_c^{-0.3} \text{ for } \mathrm{Re}_c > 300 \qquad (6)$$

For very rough surfaces, similar as for pipe flow, the drag on a RC is independent of the Reynolds number and is a function of relative roughness:[10]

$$\frac{1}{\sqrt{f_c}} = 5.76\log\left(\frac{d_c}{\varepsilon}\right) + 1.25 \qquad (7)$$

In Figure 5, the calculated shear stress is compared for SP and RC flow in the loop at 20°C. The velocity plotted on the x axis is the average cross-section velocity ($v_p = Q_p/A_p$ where Q_p is the volumetric flow rate in m^3/s and A_p is the pipe cross section in m^2) for SP flow and the RC peripheral velocity ($v_c = \omega d_c/2$) for the RC. The smooth surface correlations were used to calculate the shear stress. This was justifiable because the surface roughness varied from $\varepsilon/d_p \approx 1 \times 10^{-4}$ for the freshly polished specimens to $\varepsilon/d_p \approx 4 \times 10^{-4}$ for heavily corroded surfaces (as determined by looking at the surface cross section using SEM). Calculated from the previous correlations, even for the highest velocities, the effect of maximum roughness on shear stress was < 10%.

From Figure 5, it could be concluded that, with the RC, shear stresses up to 25 Pa could be achieved at maximum rotation speed (5,000 rpm, which corresponded to v_c = 2.61 m/s). In the SP, as much as 300 Pa was achieved at v_p = 12 m/s. For the "equal" velocity ($v_p = v_c$), similar shear stress was obtained for the two flow geometries. This will hold true only when the RC and SP diameters are of the same order of magnitude, as in the present case. Most of the present experiments were conducted at 2 m/s, where the calculated shear stress was 16 Pa and 12 Pa for the RC and the SP, respectively.

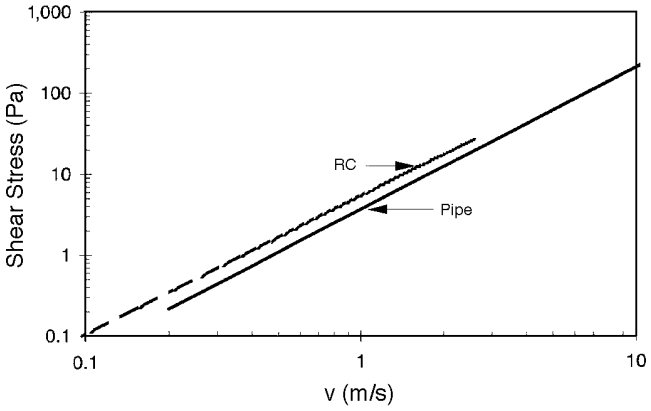

FIGURE 5. *Calculated shear stress as a function of v at T = 20°C, d_c = 0.01 m, d_p = 15 mm (0.59 in.).*

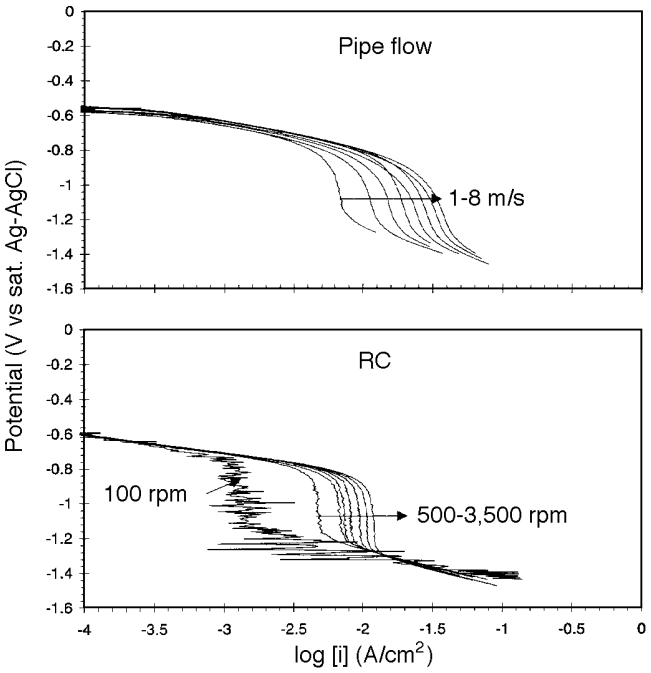

FIGURE 6. *Potentiodynamic sweep; effect of v on mass-transfer limiting currents; water, 1% NaCl solution, pH 3, T = 20°C, P_{N2} = 1 bar, p_{total} = 1 bar.*

Mass Transfer

According to general understanding of the CO_2 corrosion mechanisms, mass transfer is important primarily at pH < 5, when it affects the limiting currents for H^+ reduction. Since this pH range is in the domain of the present work, mass-transfer characterization of the two flow geometries in the loop was done.

This was achieved by conducting experiments at pH 3 in a 1% NaCl water solution purged with nitrogen gas (N_2). Under these conditions, the dominant cathodic reaction for modest overpotentials ($\eta < -0.5$ V, where η is the overpotential in V) was the reduction of H^+ ions. For overpotentials between $-0.2 < \eta < -0.5$ V, it was possible to obtain clear mass-transfer limiting currents (Figure 6). Potentiodynamic sweeps were conducted beginning from the corrosion potential and finishing 0.8 V below. This

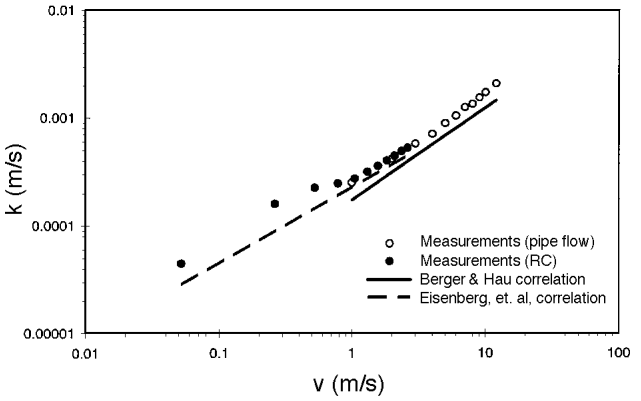

FIGURE 7. *Measured and predicted mass transfer coefficient as a function of v for the two flow geometries; T = 20°C, d_c = 0.01 m, d_p = 15 mm (0.59 in.).*

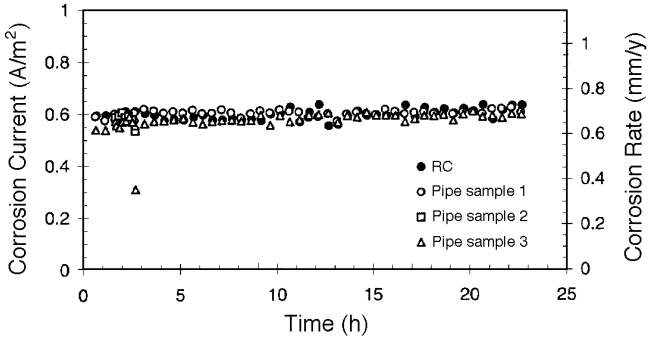

FIGURE 8. *Corrosion rate vs time followed from beginning of the experiment at T = 20°C and equivalent mass-transfer conditions: v_p = 2 m/s, v_c = 2 m/s (3,820 rpm); water, 1% NaCl, pH 5, P_{CO_2} = 1 bar, P_{total} = 1 bar; ○, □, Δ – pipe flow; ● – RC.*

was repeated for different SP velocities and RC speeds. The measured limiting currents were converted to the mass-transfer coefficient by using:

$$k_m = \frac{i^d_{lim\,(H^+)}}{F \times 10^{-pH}} \qquad (8)$$

where k_m is the mass transfer coefficient in m/s, i^d_{lim} is the diffusion limiting current density in A/m², and F is the Faraday constant (96,490 coul/equiv).

Mass-transfer coefficients for turbulent flow are well established in the literature for the two flow geometries under investigation. In the case of SP flow, the correlation of Berger and Hau could be used:[21]

$$Sh_p = \frac{k_m d_p}{D} = 0.0165 \times Re_p^{0.86} \times Sc^{0.33} \qquad (9)$$

where Sh is the Sherwood number, D is the diffusion coefficient in m²/s, and Sc is the Schmidt number.

For the RC flow the correlation of Eisenberg, et al., was appropriate:[22]

$$Sh_c = \frac{k_m d_c}{D} = 0.0791 \times Re_c^{0.7} \times Sc^{0.356} \qquad (10)$$

The measured and calculated mass-transfer coefficients as a function of velocity are shown in Figure 7. The value $D_{(H^+)} = 9.31 \times 10^{-9}$ m²/s was been used to obtain k_m from the Sherwood number.[23] In Figure 7, it was again arbitrarily selected to compare k_m for the matched velocity ($v_p = v_c$). However, the most important conclusion was that, for the RC and for the SP flow, the agreement between the measured mass-transfer coefficient in the present loop and the one predicted using the previous correlations was good. This meant that good control of the mass-transfer conditions was achieved in the loop for both flow geometries. A somewhat larger discrepancy between predicted and measured k_m was obtained for the SP flow. The working electrodes in the SP test section (Figure 2) were only 20 mm (0.787 in.) long (1.33 x d_p), and it could be assumed they were too short to eliminate the effect of developing mass-transfer boundary layers completely.

The mass-transfer measurements enabled selection of the velocity in the SP and the corresponding rotating speed for the RC, which gave identical mass-transfer rates for the two geometries.[24-25] By selecting $v_p = v_c$ = 2 m/s, practically identical mass-transfer coefficients $(k_m)_p = (k_m)_c \approx 4 \times 10^{-4}$ m/s were measured at 20°C. This was approximately in the middle of the region where the two curves overlapped (Figure 7). The majority of the conducted CO_2 corrosion experiments presented below were done at $v_p = v_c$ = 2 m/s (3,820 rpm), where the mass-transfer conditions were approximately equal.

CO_2 Corrosion

Corrosion experiments were carried out over a wide range of parameters: T = 20°C to 80°C, pH = 4 to 6, P_{CO_2} = 1 bar (100 kPa), and v = 0 m/s to 13 m/s. Experiments were started by measuring the polarization resistance (corrosion rate) every 30 min at $v_p = v_c$ = 2 m/s (matching mass-transfer conditions). In most of the experiments, a stable corrosion rate was observed (Figure 8). In this experiment, good agreement was obtained between the corrosion rates for the RC and SP specimens.

Typically 24 h after the beginning of the experiments, measurements of the polarization resistance (corrosion rate) and the corrosion potential as a function of velocity were performed. The velocity was varied from 0 m/s to 13 m/s and back in the SP section and from 0 rpm to 5,000 rpm and back in the RC chamber.

Subsequently, velocity was adjusted back to $v_p = v_c$ = 2 m/s. After a waiting period of 12 h (to obtain

stable corrosion rates), AC impedance measurements were conducted. Finally, potentiodynamic sweeps were done, and the specimens were taken out from the loop and prepared for SEM analysis.

Experiments at 20°C — The potentiodynamic sweeps measured at $v_p = v_c = 2$ m/s (equivalent mass-transfer conditions) and different pH are shown in Figure 9. The measured curves are overlaid with theoretical curves predicted with the model of Nešić, et al., for easier interpretation of the corrosion mechanisms.[11] The data obtained for the RC electrode were in good agreement with data from the SP section over the whole potential range for all three pH. At pH 4, a large contribution of the H^+ reduction reaction could be seen. This contribution diminished at pH 5 and completely disappeared at pH 6. At pH 5 and 6, the dominant cathodic reaction at the corrosion potential was direct H_2CO_3 reduction, and for higher negative overpotentials, the dominant cathodic reaction was H_2O reduction. Good agreement between the RC and SP measurements was clear for all three cathodic reactions, as well as for the anodic reactions. This led to a conclusion that the mechanism of the CO_2 corrosion in the two flow geometries (RC and SP) was the same at 20°C. It then was not difficult to understand that the measured corrosion rates shown in Figure 8 were very similar for the two geometries.

The potentiodynamic sweeps shown in Figure 9 were corrected for the solution resistance found by the AC impedance technique. In Figure 10, results of the AC impedance measurements (Nyquist plot) at 20°C, pH = 6, and $v_p = v_c = 2$ m/s are shown. A good agreement between the measured polarization resistance values for the RC and SP geometry was evident. Taking into account the difference in area for the two sample geometries (10% larger for the RC), the measured polarization resistances in Ω-m² for the two geometries were even closer. The similar shape of the measured curves confirmed that an identical mechanism of CO_2 corrosion was present in both flow geometries.

The obtained corrosion rates as a function of velocity at 20°C are shown in Figure 11 for the different pH.[(3)] The corrosion current is shown on the left and the corresponding corrosion rate on the right side (for iron dissolution, the relation 1 mm/y = 1.155 A/m² was used). The corrosion rates at static conditions were approximately the same for all three pH values, as were the corrosion potentials (Figure 12). The only difference in the corrosion rates for the three different pH values came from the H^+ reduction reaction. However, in static conditions, the mass-transfer limiting current for H^+ reduction was very small in all three cases, so the chemical reaction-controlled reduction of H_2CO_3 was the dominant cathodic reaction.

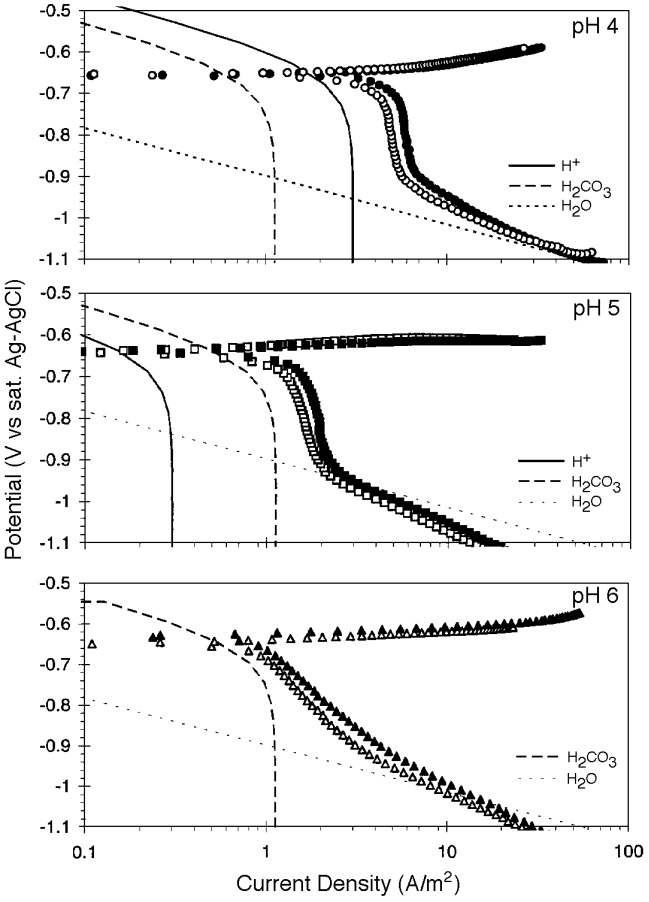

FIGURE 9. *Potentiodynamic sweeps for different pH values conducted at T = 20°C and equivalent mass-transfer conditions: $v_p = v_c = 2$ m/s (3,820 rpm); water, 1% NaCl, $P_{CO_2} = 1$ bar, $P_{total} = 1$ bar; ○, □, Δ – pipe flow; ●, ■, ▲ – RC.*

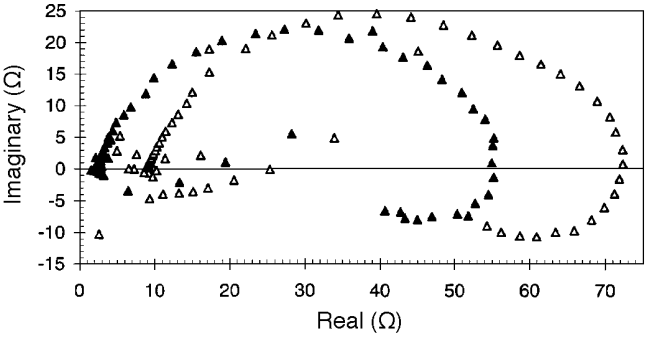

FIGURE 10. *AC impedance measurement at T = 20°C, pH 6 and equivalent mass-transfer conditions: $v_p = v_c = 2$ m/s (3,820 rpm); water, 1% NaCl, $P_{CO_2} = 1$ bar, $P_{total} = 1$ bar; Δ – pipe flow; ▲ – RC.*

[(3)] In this and in all subsequent figures where the effect of velocity has been shown, the results were corrected for the effect of the presence of oxygen by subtracting the contribution of the oxygen reduction current. Measured oxygen concentrations varied from 10 ppb to 40 ppb in different experiments. Previously shown mass-transfer correlations and the diffusion coefficient (D_{O_2} = 2.09 x 10^{-9} m²/s at 20°C) were used to calculate the limiting currents for oxygen reduction.

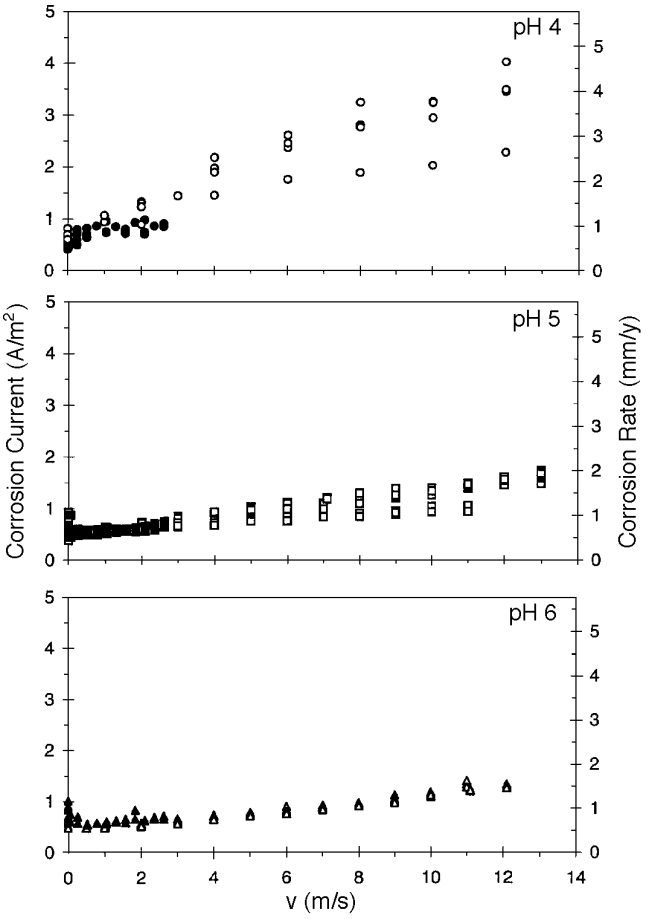

FIGURE 11. *Effect of v on the corrosion rate at different pH values and T = 20°C; water, 1% NaCl, P_{CO_2} = 1 bar, P_{total} = 1 bar; ○, □, Δ – pipe flow; ●, ■, ▲ – RC.*

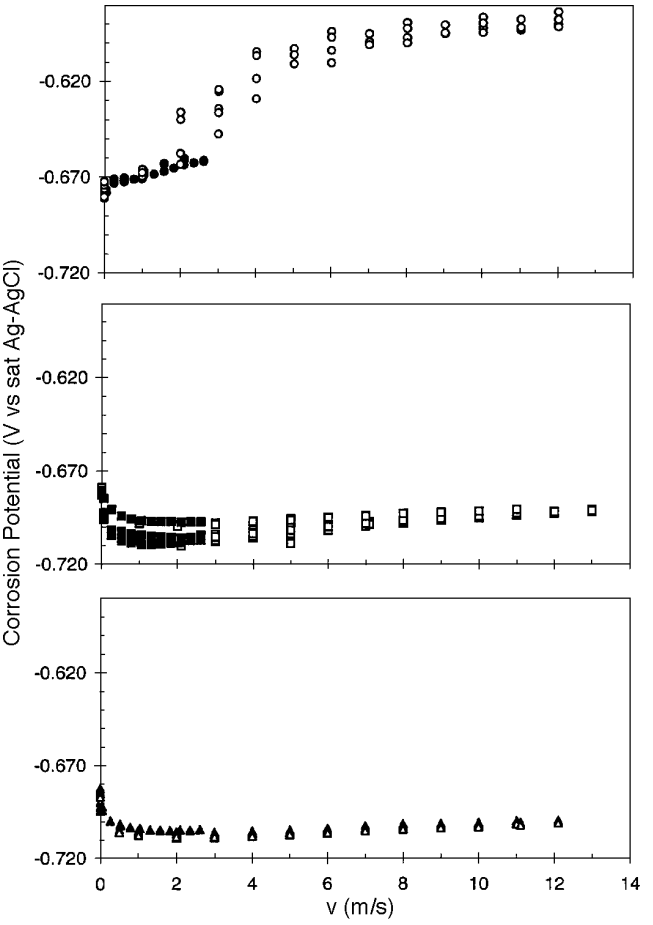

FIGURE 12. *Effect of v on the corrosion potential at different pH values and T = 20°C; water, 1% NaCl, P_{CO_2} = 1 bar, P_{total} = 1 bar; ○, □, Δ – pipe flow; ●, ■, ▲ – RC.*

As velocity was increased, the limiting current for H^+ reduction increased, leading to an increased overall cathodic reaction and higher corrosion rate. The increase of the corrosion rate with velocity was most pronounced at pH 4, where the concentration of H^+ was highest. At pH 4, already at 1 m/s, the contributions of H^+ reduction and H_2CO_3 reduction were equal (Figure 4). For higher velocities, the flow-dependent H^+ reduction dominated. At pH 5 and 1 m/s, the H^+ reduction was only 10% of the overall cathodic reaction, while at 10 m/s,the H^+ and H_2CO_3 reduction were of the same order of magnitude. Thus, the increase in corrosion rate as a function of velocity at pH 5 still could be explained by the increasing contribution of mass transfer-controlled H^+ reduction. However, this was not the case for pH 6.

At pH 6, there were so few H^+ ions that, even at the highest velocity tested, they give a small contribution to the overall cathodic current (10% at 10 m/s). To explain the observed doubling in the corrosion rate when the velocity changed from 1 m/s to 12 m/s, another flow-dependent reaction had to be identified. It was proposed that the higher cathodic current observed at higher velocities (pH 6) came from an accelerated H_2CO_3 reduction reaction. In other words, it was proposed that there was a diffusion-controlled component of the H_2CO_3 limiting current in addition to the chemical reaction-controlled component, as already proposed by Schmitt and Rothman.[14] The concept of pure chemical reaction-controlled limiting current is strictly valid only when the thickness of the mass-transfer boundary layer is much larger than the thickness of the "reaction" layer.[26] As a first approximation, it could be said that this is correct at higher temperatures and low velocities. In the present case (pH 6, high velocity, and low temperature), in addition to the H_2CO_3 being formed by the slow hydration step near the metal surface, significant amounts of H_2CO_3 were transported by diffusion from the bulk. This meant that the limiting current for H_2CO_3 generally had two components: a flow-independent (chemical reaction-controlled) part and a flow-dependent (mass

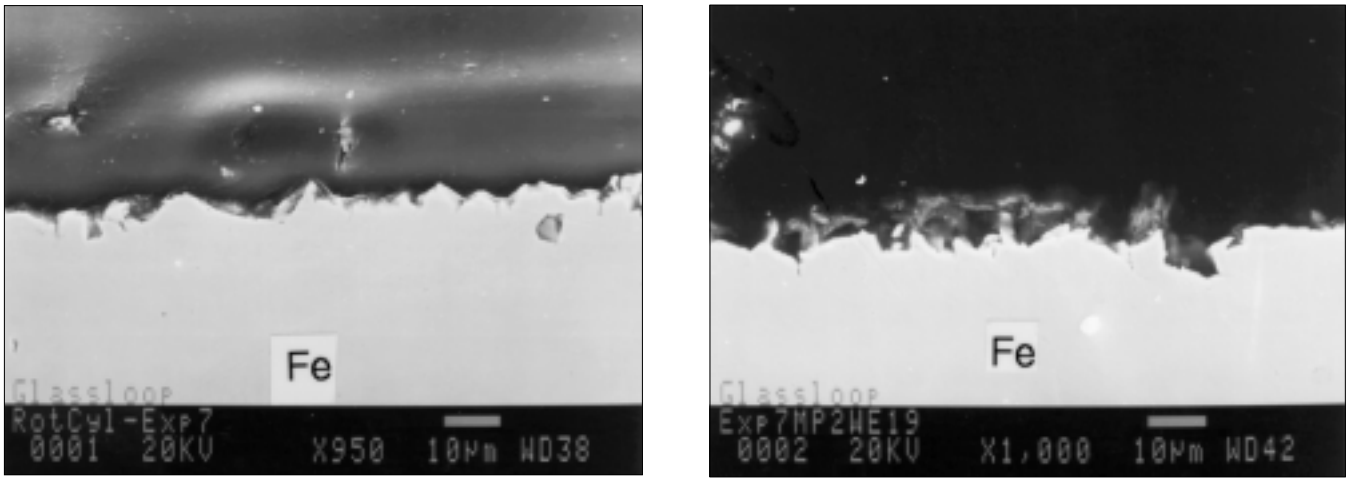

(a) (b)

FIGURE 13. *SEM images of the cross section of the corroded surfaces exposed for 63 h at T = 20°C, pH 5 and equivalent mass-transfer conditions: $v_p = v_c = 2$ m/s (3,820 rpm); water, 1% NaCl, $P_{CO_2} = 1$ bar, $P_{total} = 1$ bar; (a) RC specimen and (b) SP specimen.*

transfer-controlled) part. A detailed theoretical treatment of this concept will be published in the future.

Figure 11 shows good agreement obtained for the corrosion rates of the RC and SP specimens. The same was true for the measured corrosion potentials (Figure 12). This suggested that, in the absence of surface films, identical corrosion rates could be obtained by setting equivalent water chemistry and mass-transfer conditions at the two flow geometries. It also confirmed that, in this case, the present understanding of CO_2 corrosion mechanisms permitted the transfer the data from one flow system to another.

In Figure 13, SEM images of the cross sections of a specimen exposed for 63 h at 20°C and pH 5 are shown. An evenly attacked surface virtually free of any films was evident.

Experiments at 50°C — Potentiodynamic sweeps measured at 50°C, pH 4, and $v_p = v_c = 2$ m/s (equivalent mass-transfer conditions) are shown in Figure 14. A higher rate of the overall cathodic reaction was observed over the whole range of negative overpotentials for the RC electrode compared to the SP. The difference between the anodic reactions seemed to be smaller. However, it was difficult to judge this because of the low slope of the anodic lines.

It was no surprise then that the velocity test done in the same experiment failed to show good agreement between the RC and SP curves (Figure 14). The shape of the measured curves (Figure 15) was similar for the two geometries, suggesting a similar corrosion mechanism. The same conclusion could be reached by looking at the AC impedance measurements conducted in the same experiment (Figure 16). Similar results were obtained in experiments conducted at pH 5 and pH 6 at the same temperature.

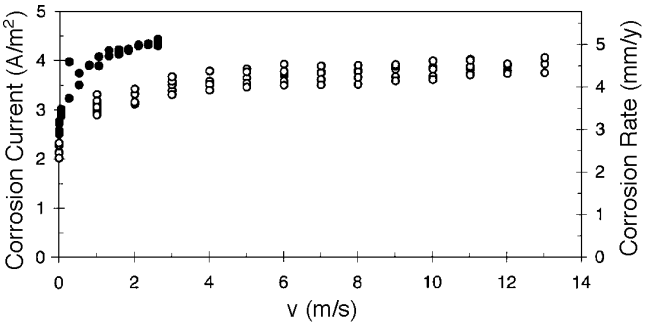

FIGURE 14. *Effect of v on the corrosion rate at T = 50°C, pH 4 and equivalent mass-transfer conditions water; 1% NaCl, $P_{CO_2} = 1$ bar, $P_{total} = 1$ bar; ○ – pipe flow; ● – RC.*

It initially was difficult to explain why the good agreement between the two flow systems found at 20°C was not obtained again at 50°C until SEM images of the corroded surfaces cross section were analyzed. In both cases (SP and RC specimens), there were films on the surfaces (Figure 17). The film found on the RC specimen (Figure 17[a]) was more porous, consisting primarily of iron carbide (uncorroded part of the steel) and probably presented a very weak diffusion barrier for the corroding species. The film found on the surface of the SP specimen (Figure 17[b]) was more dense, consisting of an iron carbide matrix filled partially with iron carbonate. This film looked laminated and fractured (which probably occurred during drying). However, it could be assumed that it acted as a stronger diffusion barrier. The previous observations helped explain the discrepancy in the electrochemical measurements

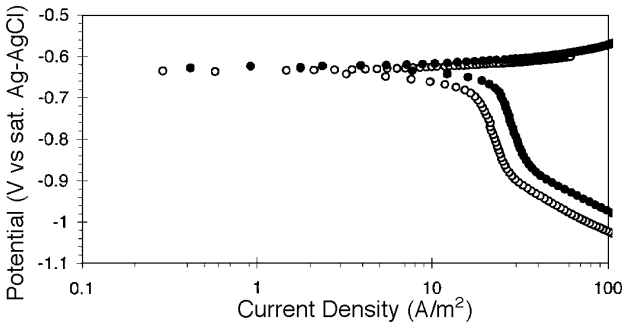

FIGURE 15. *Potentiodynamic sweep conducted at T = 50°C, pH 4 and equivalent mass-transfer conditions: $v_p = v_c = 2$ m/s (3,820 rpm); water, 1% NaCl, $P_{CO_2} = 1$ bar, $P_{total} = 1$ bar; ○ – pipe flow; ● – RC.*

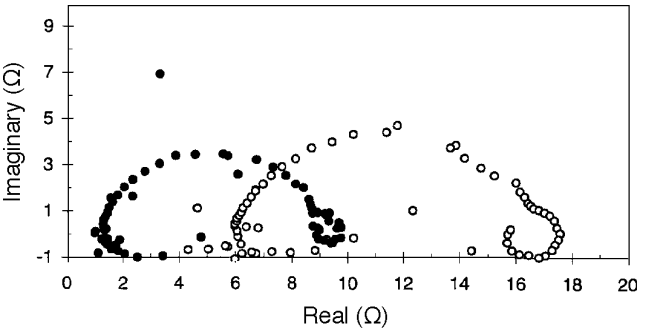

FIGURE 16. *AC impedance measurement at T = 50°C, pH 4 and equivalent mass-transfer conditions: $v_p = v_c = 2$ m/s (3,820 rpm); water, 1% NaCl, $P_{CO_2} = 1$ bar, $P_{total} = 1$ bar; ○ – pipe flow; ● – RC.*

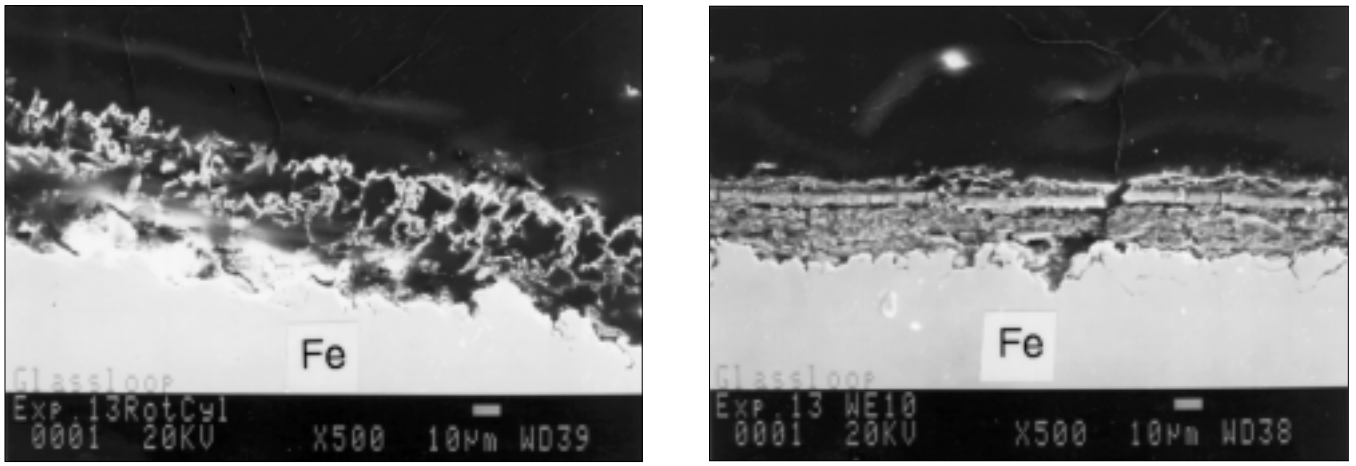

(a) (b)

FIGURE 17. *SEM images of the cross section of the corroded surfaces exposed for 175 h at T = 50°C, pH 4 and equivalent mass-transfer conditions: $v_p = v_c = 2$ m/s (3,820 rpm); water, 1% NaCl, $P_{CO_2} = 1$ bar, $P_{total} = 1$ bar; (a) RC specimen and (b) SP specimen.*

shown in Figures 14 and 15. It could be concluded that more dense (protective[4]) films formed on the SP specimen compared to the RC specimen at 50°C.

The question to be answered was how the protective films formed in the first place. It is known that, at pH 4, the solubility of iron carbonate is quite high (much higher than measured values in the present experiments) and that the likelihood of forming protective films is low.[27] However, since iron carbide films were formed, they could have created more favorable conditions at the steel surface for iron carbonate precipitation. This was aided by the higher temperatures (50°C) that accelerated the precipitation of iron carbonate.[27]

The next question was why more dense and protective films formed on the SP steel electrode. The difference between the two flow systems was a small pressure gradient that existed at the RC electrode and came from the centrifugal force acting in the direction perpendicular to the steel surface. It was estimated roughly that the difference between pressure at the surface of the RC and the bulk pressure was of the order of 1 Pa in these experiments. In addition, the calculated shear stress at the RC electrode was a few Pa higher than the one in the SP for the same mass-transfer conditions ($v_p = v_c = 2$ m/s) in the present loop (Figure 5). Finally, a small centrifugal force acting on the forming solid film which was present at the RC did not exist in the SP flow. It only could be speculated that these very mild forces were responsible for noticeably different film structures at the two flow geometries.

Experiments at 80°C — At 80°C, similar results were obtained as for 50°C. The difference between the RC and SP specimens was even more pronounced

[4] Surface films that enable corrosion rates of several mm/y could hardly be called protective in a practical sense. However, they do act as a diffusion barrier and reduce corrosion.

at 80°C (Figure 18). The potentiodynamic sweep done at 80°C, pH 4, and $v_p = v_c = 2$ m/s (equivalent mass-transfer conditions) showed once again that it was easier to notice the difference in the corrosion process for the two flow geometries on the cathodic reactions. The AC impedance measurements (Figure 19) suggested a similar corrosion mechanism for the two geometries and the presence of a diffusion-controlled process in both cases. This further reinforced our hypothesis that protective films were responsible for the observed differences in CO_2 corrosion at the RC and SP specimens. By looking at the SEM images of the cross section of specimens from the same experiment exposed for 70 h (Figure 20), films could be noticed with an iron carbide porous structure and dense iron carbonate precipitates in between. Again, the films formed on the RC specimen looked more porous and less protective than the films formed on the SP specimen.

Despite the presence of surface films, a significant increase was evident in the rate of the overall cathodic reactions at higher temperatures (50°C and 80°C) as shown in Figures 15 and 18. Surprisingly, the anodic reactions were not accelerated significantly at higher temperatures. This apparent anomaly will be the subject of more detailed investigation.

In general, the corrosion rate was higher at higher temperatures. It could be noticed further that the flow dependence of the corrosion rate was less pronounced at higher temperature (Figures 11, 14, and 21). This was contrary to what Eriksrud and Søndvedt reported previously.[15] The present findings could be explained by remembering that flow dependence comes from the mass-transfer limiting currents. At higher temperatures, the chemical reaction-controlled limiting current for H_2CO_3 reduction dominated as it was accelerated more rapidly than the diffusion limiting currents for H^+ and H_2CO_3 reduction. The overall corrosion process, which was under partial mass-transfer control at lower temperatures (20°C), changed to a mixed charge transfer/chemical reaction control at higher temperatures (50°C and 80°C). The surface films which formed and acted as a mass-transfer barrier also could have been partially responsible for the observed lack of flow dependence at higher temperatures.

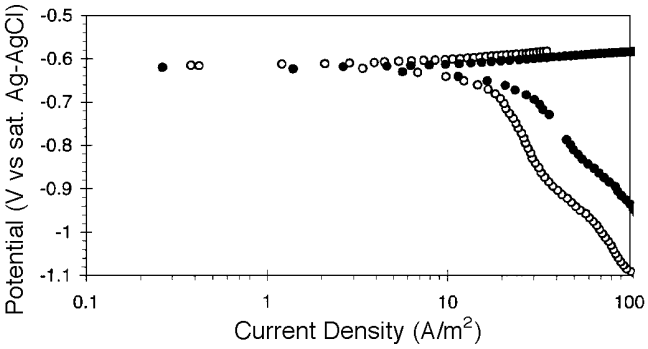

FIGURE 18. *Potentiodynamic sweep conducted at T = 80°C, pH 4 and equivalent mass-transfer conditions: $v_p = v_c = 2$ m/s (3,820 rpm); water, 1% NaCl, $P_{CO_2} = 1$ bar, $P_{total} = 1$ bar; ○ – pipe flow; ● – RC.*

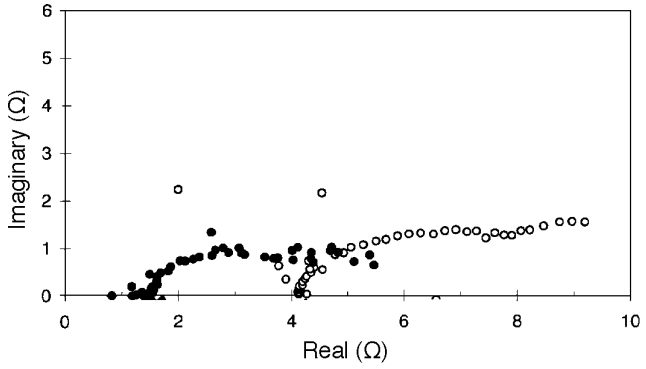

FIGURE 19. *AC impedance measurement at T = 80°C, pH 4 and equivalent mass-transfer conditions: $v_p = v_c = 2$ m/s (3,820 rpm); water, 1% NaCl, $P_{CO_2} = 1$ bar, $P_{total} = 1$ bar; ○ – pipe flow; ● – RC.*

CONCLUSIONS

❖ Good agreement was obtained between the measured mass-transfer coefficients and the ones predicted using the correlation of Berger and Hau[21] for SP flow and the correlation of Eisenberg, et al.,[22] for the RC flow geometry. This enabled selection of a velocity in the pipe and the corresponding rotating speed for the RC, which gave approximately equal mass-transfer conditions for the two geometries.

❖ Flow-dependent CO_2 corrosion rates at pH 4 and 5 and 20°C were obtained that could be explained by the flow-dependent mass-transfer limiting current for H^+ ions. The observed flow dependence at pH 6 and 20°C could not be explained with the mass-transfer limitation of H^+ ions. It was proposed that there was a diffusion-controlled component of H_2CO_3 limiting current, in addition to the chemical reaction-controlled component, as previously proposed by Schmitt and Rothman.[14]

❖ A significant increase in the corrosion rate at higher temperatures (50°C and 80°C) was obtained as a consequence of the increased rate of the overall cathodic reactions. It was observed that the anodic reactions were not accelerated significantly at higher temperatures.

❖ The flow dependence of the corrosion rate was less pronounced with increasing temperature because of the change in the corrosion mechanism from mixed charge/mass-transfer control at low temperature (20°C) to mixed charge transfer/chemical reaction control at higher temperatures (50°C and 80°C). At higher temperatures, the chemical reaction-controlled limiting current for H_2CO_3 reduction was

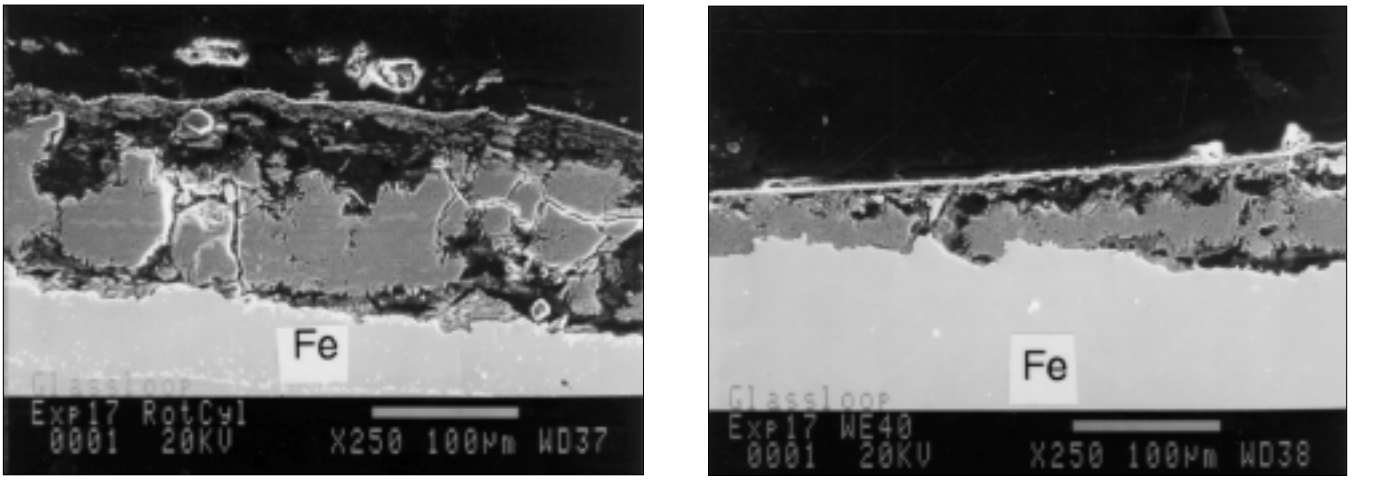

(a) (b)

FIGURE 20. *SEM images of the cross section of the corroded surfaces exposed for 170 h at T = 80°C, pH 4 and equivalent mass transfer-conditions: $v_p = v_c = 2$ m/s (3,820 rpm); water, 1% NaCl, $P_{CO_2} = 1$ bar, $P_{total} = 1$ bar; (a) RC specimen and (b) SP specimen.*

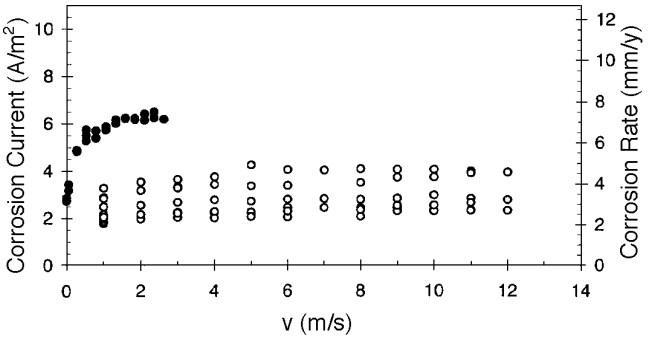

FIGURE 21. *Effect of v on the corrosion rate at T = 80°C, pH 4 and equivalent mass-transfer conditions; water, 1% NaCl, $P_{CO_2} = 1$ bar, $P_{total} = 1$ bar; ○ – pipe flow; ● – RC.*

accelerated more rapidly than the diffusion limiting currents for H^+ and H_2CO_3 reduction.

❖ At higher temperatures (50°C and 80°C), films formed on the metal surface and acted as a mass-transfer barrier that somewhat reduced the corrosion rate. In general, more dense and protective films formed on the SP specimen compared to the RC specimen. It was speculated that the somewhat higher shear stress and a small radial pressure gradient at the RC electrode were responsible for noticeably different film structures at the two flow geometries. The surface films also could have been partially responsible for the observed lack of flow dependence at higher temperatures.

❖ In the absence of surface films, it was possible to achieve the same mechanism and obtain approximately the same rate of the CO_2 corrosion process at a RC as at a SP electrode by setting identical water chemistry and mass-transfer conditions at the two flow geometries. This confirmed that the present understanding of CO_2 corrosion mechanisms in the absence of surface films permitted the transfer of data from one flow system to another and ultimately to the field.

ACKNOWLEDGMENTS

This work was supported financially by Statoil.

LIST OF SYMBOLS

A	area	(m^2)
d_p, d_c	pipe and cylinder diam)	(m)
D	diffusion coefficient	(m^2/s)
$f = 2\tau_w/\rho v^2$	Fanning friction factor	
F	Faraday constant	(96,490 coul/equiv.)
i	current density	(A/m^2)
i^d_{lim}	diffusion limiting current density	(A/m^2)
k_m	mass-transfer coefficient	(m/s)
l	characteristic length	(m)
L	pipe length	(m)
p	pressure	(bar)
P_{CO_2}	partial pressure of CO_2	(bar)
Q	volumetric flow rate	(m^3/s)
R	universal gas constant	(8.3143 J/[mol K])
$Re = \rho v l/\mu$	Reynolds number	
$Sc = \mu/\rho D$	Schmidt number	
$Sh = k_m l/D$	Sherwood number	
T	temperature	(°C)
v	velocity	(m/s)

Greek Symbols

ε	pipe roughness	(m)
ν	viscosity	(kg/m-s)

ρ	density	(kg/m^3)
τ_w	wall shear stress	(Pa)
ω	rotation (angular) speed	(rad/s)

Subscripts

p	pipe
c	cylinder

REFERENCES

1. K.D. Efird, Corrosion 33 (1977): p. 3.
2. S. Nešić, J. Postlethwaite, Corrosion 46 (1990): p. 874.
3. L.W. Shemilt, C.Y. Cha, E. Fiadzigbe, A.B. Ponter, Corros. Sci. 20 (1980): p. 443.
4. D.C. Silverman, "Rotating Cylinder Electrode — An Approach for Predicting Velocity-Sensitive Corrosion," CORROSION/90, paper no. 13 (Houston, TX: NACE, 1990).
5. K. Denpo, H. Ogawa, "Fluid Flow Effects on Corrosion Resistance of Oil-Well Materials," CORROSION/90, paper no. 28 (Houston, TX: NACE, 1993).
6. K.D. Efird, E.J. Wright, J.A. Boros, T.G. Hailey, "Experimental Correlation of Steel Corrosion in Pipe Flow with Jet Impingement and Rotating Cylinder Laboratory Tests," CORROSION/93, paper no. 91 (Houston, TX: NACE, 1993).
7. H. Schlichting, Boundary-Layer Theory, 7th ed., translation from German (New York, NY: McGraw-Hill, 1987).
8. V.G. Levich, Physicochemical Hydrodynamics, translation from Russian (Englewood Cliffs, NJ: Prentice-Hall Inc., 1962), p. 60.
9. D.R. Gabe, J. Appl. Electrochem. 4 (1974): p. 91.
10. D.R. Gabe, F.C. Walsh, J. Appl. Electrochem. 13 (1983): p. 3.
11. S. Nešić, J. Postlethwaite, S. Olsen, "An Electrochemical Model for Prediction of CO_2 Corrosion," CORROSION/95, paper no. 131 (Houston, TX: NACE, 1995).
12. M. Stern, J. Electrochem. Soc. 102 (1955): p. 609.
13. C. deWaard, D.E. Milliams, Corrosion 31 (1975): p. 131.
14. G. Schmitt, B. Rothman, Werkst. Korros. 28 (1977): p. 816.
15. E. Eriksrud, T. Søntvedt, "Effect of Flow on CO_2 Corrosion Rates in Real and Synthetic Formation Waters," in Advances in CO_2 Corrosion, vol. 1, Proc. CORROSION/83 Symp. CO_2 Corrosion in the Oil and Gas Industry, eds. R.H. Hausler, H.P. Goddard (Houston, TX: NACE, 1984), p. 20.
16. P. Delahay, J. Amer. Chem. Soc. 74 (1952): p. 3,497.
17. L.G.S. Gray, B.G. Anderson, M.J. Danysh, P.G. Tremaine, "Mechanism of Carbon Steel Corrosion in Brines Containing Dissolved Carbon Dioxide at pH 4," CORROSION/89, paper no. 464 (Houston, TX: NACE, 1989).
18. J.O'M. Bockris, D. Drazic, A.R. Despic, Electrochim. Acta 4 (1961): p. 325.
19. K. Videm, "Fundamental Studies aimed at Improving Models for Prediction of CO_2 Corrosion," in Progress in the Understanding and Prevention of Corrosion, Proc. 10th European Corros. Cong., vol. 1 (London, England: Institute of Metals, 1993), p. 513.
20. Perry's Chemical Engineers' Handbook, 6th ed. (New York, NY: McGraw-Hill, 1984), p. 5-23.
21. F.P. Berger, K.-F. F.-L Hau, Int. J. Heat Mass Transfer 20 (1977): p. 1,185.
22. M. Eisenberg, C.W. Tobias, C.R. Wilke, J. Electrochem. Soc. 101 (1954): p. 306.
23. P.W. Atkins, Physical Chemistry, 2nd ed. (Oxford, UK: Oxford University Press, 1982), p. 905.
24. V.E. Heitz, Werkst. Korros. (1964): p. 63.
25. T. Chen, A.A. Moccari, D.D. Macdonald, "The Development of Controlled Hydrodynamic Techniques for Corrosion Testing," CORROSION/91, paper no. 292 (Houston, TX: NACE, 1991).
26. K.J. Vetter, "Electrochemical Kinetics, Theoretical Aspects," in Electrochemical Kinetics: Theoretical and Experimental Aspects, translation from German (New York, NY: Academic Press, 1967), p. 235.
27. A. Dugstad, "Importance of $FeCO_3$ Supersaturation on the CO_2 Corrosion of Carbon Steel," CORROSION/92, paper no. 14 (Houston, TX: NACE, 1992).